Collocation of Geostationary Satellites Using Convex Optimization

Frederik J. de Bruijn[1] and Stephan Theil[2]
Institute of Space Systems, German Aerospace Center (DLR),

Robert-Hooke-Strasse 7, 28359 Bremen, Germany

Daniel Choukroun[3]
Ben Gurion University of the Negev, POB 653, 84105, Beer-Sheva, Israel

Eberhard Gill[4]
Faculty of Aerospace Engineering, Delft University of Technology,

Kluyverweg 1, 2629 HS Delft, The Netherlands

A method is developed to determine station-keeping maneuvers for a fleet of satellites collocated in a geostationary slot. The method is enabled by a linear time-varying formulation of the satellite orbit dynamics in terms of non-singular orbital elements. A leader-follower control hierarchy is used, such that the motion of the follower satellites is controlled relative to the leader. Key objectives of the station-keeping method are to minimize propellant consumption and to limit the number of maneuvers, while guaranteeing safe separation between the satellites. The method is applied in a realistic simulation scenario, including orbit determination, actuation and modeling errors. The method is demonstrated to work for fleet of four satellites with differences in mass, surface area and propulsion system for a maneuver cycle of one week. It is then demonstrated that by reducing the maneuver cycle duration to one day, the method allows to collocate 16 satellites in a single slot, without penalties on propellant consumption.

---

[1] Researcher, Department of GNC Systems
[2] Department head, Department of GNC Systems
[3] Senior Lecturer, Mechanical Engineering Department
[4] Professor and Chairholder, Department of Space Systems Engineering

Nomenclature

α	Right ascension of geostationary position [rad]
$\Delta\mathbf{e}$	Relative eccentricity vector $\Delta\mathbf{e} = (\Delta e_x, \Delta e_y)^T$ [-]
$\Delta\mathbf{i}$	Relative inclination vector $\Delta\mathbf{i} = (\Delta i_x, \Delta i_y)^T$ [rad]
Δe	Relative eccentricity [-]
δe	Magnitude of relative eccentricity vector [-]
Δi	Relative inclination [rad]
δi	Magnitude of relative inclination vector [rad]
ΔL	Relative mean longitude [rad]
δM	Angle between satellite position and relative eccentricity vector [rad]
Δn	Relative mean orbital motion [rad/s]
$\delta\Omega$	Phase angle of relative inclination vector [rad]
$\delta\omega$	Angle between relative eccentricity and inclination vectors [rad]
$\delta\tilde{\omega}$	Phase angle of relative eccentricity vector [rad]
Γ	Thruster configuration matrix mapping thrusts to RTN frame
$\{.\}^i$	Superscript i refers to i^{th} Follower satellite
$\{.\}^L$	Superscript L refers to Leader satellite
$\{.\}_{\text{GEO}}$	Subscript GEO refers to a geostationary orbit
$\{.\}_{lb}$	Subscript lb refers to lower bound
$\{.\}_{ub}$	Subscript ub refers to upper bound
$\mathbf{e}$	Eccentricity vector $\mathbf{e} = (e_x, e_y)^T$ [-]
$\mathbf{i}$	Inclination vector $\mathbf{i} = (i_x, i_y)^T$ [rad]
$\mathbf{T}$	Thrust force vector [N]

$\mathbf{u}_c$	Vector of controlled accelerations in RTN frame [m/s^2]
$\mathbf{u}_d$	Vector of disturbing accelerations in RTN frame [m/s^2]
μ_E	Gravitational parameter Earth [m^3/s^2]
Ω	Right ascension of ascending node [rad]
ω	Argument of perigee [rad]
ρ	Magnitude of relative position vector [m]
$\tilde{\omega}$	$\tilde{\omega} = \omega + \Omega$ [rad]
ε	Mean longitude at epoch t_0 $L = \omega + \Omega + M_0$ [rad]
a	Semi-major axis [m]
e	Eccentricity [-]
i	Inclination [rad]
L	Argument of mean longitude $L = \omega + \Omega + M$ [rad]
M	Mean anomaly [rad]
m	Satellite mass [kg]
n	Mean orbital motion [rad/s]
n_E	Mean angular rate Earth [rad/s]
r_e	Radius of relative eccentricity vector control window [-]
r_i	Radius of relative eccentricity vector control window [rad]
S_e	Set describing relative eccentricity vector control window
S_i	Set describing relative inclination vector control window
V	Satellite velocity [m/s]
x, y, z	Components of relative position vector in radial, tangential and normal direction [m]

I. Introduction

Syncom II was launched in 1963 and was the first satellite to arrive in a geosynchronous orbit. Since that time many satellites followed, and the geostationary orbit (GEO) in particular has

become increasingly populated due to the high economic and political value of assets in this orbit. Driven by the need to avoid radio-frequency interference between different satellites, the geostationary orbit was divided into slots, which are allocated by the International Telecommunication Union. The limited availability and difficulty of obtaining these slots, especially at key locations above densely populated areas, together with the ever increasing need for geostationary satellite services lead several organizations to collocate multiple satellites within a single geostationary slot, see e.g. [1].

The problem of collocating a fleet of geostationary satellites shares many similarities to other distributed space systems, such as formations, clusters or swarms of satellites. One of the key challenges in orbit maintenance of distributed space systems is collision avoidance which is dealt with by maintaining a certain minimum separation distance between satellites. Collocation strategies developed to control more than two satellites in a geostationary slot generally rely on a technique called eccentricity / inclination (e/i) vector separation, introduced by Eckstein [2], and have been used for over 20 years to safely collocate geostationary satellites ([1]). Eccentricity and inclination vectors for geostationary satellites lie in the equatorial plane and point respectively in the direction of perigee and towards the ascending node, and have a magnitude depending on eccentricity and inclination. The key idea is to configure the satellites' desired mean eccentricity and inclination vectors such that their relative eccentricity and inclination vectors are (anti-)parallel. Such configuration uses the natural orbit dynamics to maintain safe separation distances by ensuring that radial separation is maximum when normal separation vanishes and vice-versa.

The current state-of-art in collocation of geostationary satellites uses relative orbital elements only in the definition of a desired configuration. The satellites are then controlled individually to stay close to their desired (absolute) states. Collision avoidance is treated in a reactive fashion by monitoring the (relative) motion of the satellites [3]. To minimize the required number of collision avoidance maneuvers large separations of eccentricity and inclinations vectors are required. Orbit determination errors, actuator errors, modeling errors, and the large variations of osculating eccentricity and inclination vectors all cause deviations from the desired mean eccentricity and inclination vectors, requiring large tolerance windows. This approach severely limits the number of satellites

that can be collocated in a single geostationary slot.

Research in the field of other distributed space systems has been inspired by the techniques developed for collocation of geostationary satellites. In [4] an impulsive control method based on e/i vector separation was introduced for controlling the relative motion of a formation of two low Earth orbiting satellites. The relative motion was controlled directly in terms of relative orbital elements. Relative orbital elements have in turn been investigated for controlling collocated geostationary satellites. Beigelmann and Gurfil [5] present a method for calculating collocation maneuvers using relative orbital elements under influence of the J_2 perturbation. Other dominant perturbations were omitted in their work. Rausch ([6], Chap. 4) includes also other dominant perturbations (but no sensor and actuator errors) and propose a method to calculate impulsive maneuvers to achieve desired relative orbital element differences. Constraints on relative states between subsequent maneuver calculations cannot be taken into account using such control strategy and thus relative separation distances cannot be guaranteed at every point in time (i.e. a minimum separation distance is guaranteed for the nominal configuration, but perturbations induce drift, moving the relative orbital elements away from their desired values). In addition, the impulsive maneuver assumption further limits applicability to satellites with a high thrust-to-mass ratio.

The use of numeric optimization based methods allows a more proactive approach. Constraints on maximum accelerations due to limitations of the propulsion system are straightforward to take into account. Maneuvers can be planned such that constraints on relative states are satisfied at every point in time. Maintaining a minimum separation distance imposes a non-convex constraint in Cartesian space on such numeric optimization strategy. Algorithms for formation maintenance and reconfiguration of distributed space systems managed a convexification of such constraint successfully by defining a series of halfspaces (or separating planes) at discrete timesteps using a heuristic approach [7] or by using sequential convex programming techniques where the last iteration is used to define the intersection of halfspaces that constitute the collision-safe region [8].

This paper develops a convex optimization-based method to accurately control the relative orbital elements of collocated geostationary satellites in the presence of all dominant perturbations, errors and model uncertainty. It is shown that by controlling relative orbital elements, notably

relative eccentricity and inclination vectors, inside convex control windows, minimum separation distances between satellites can be guaranteed. Defining constraint windows on relative orbital elements does not inhibit natural orbital motion and removes the need for a convexification of the minimum separation distance constraint. In [9] it was demonstrated that differential perturbations between satellites are small within a geostationary slot, suggesting that, in the absence of maneuvers, variations in the osculating relative states are small as well. Thus if the guidance and control problem is formulated directly in terms of osculating relative states, and these relative states are maintained within small tolerance windows, the number of satellites that can be collocated within a single slot increases. To achieve this increase, the method for station-keeping of geostationary satellites introduced in [9] is reformulated in terms of relative states. A leader-follower control hierarchy is used to control the fleet. The leader satellite can be controlled using any desired method (we use the method from [9]), and it is assumed that the predicted leader's state trajectory is available for determining the followers' station-keeping maneuvers. Since the follower trajectory is only dependent on the leader state trajectory, the method can be implemented in a decentralized manner and is scalable to an arbitrary number of follower satellites (n.b the number of follower satellites is limited by the size of the geostationary slot, and the desired minimum separation distance). The maneuvers are determined by formulating and solving a convex optimization problem. The method from [9] is further improved by explicitly accounting for the thruster configuration and using directly the thrusts of each individual thruster as independent variables in the optimization problem. The optimization problem is scaled to improve the numeric solution.

A simulation campaign was performed and the method is demonstrated to work under realistic (even conservative) orbit determination errors, actuator errors and modeling errors, and for satellites with different design characteristics. It is also shown that by decreasing the maneuver cycle duration, it is possible to collocate a larger number of satellites in a slot. A demonstration of the method is given for four satellites, for a maneuver cycle duration of 7 days, and for a fleet of 16 satellites for a maneuver cycle duration of 1 day. Results are analyzed in terms of propellant consumption, number of maneuvers, accuracy of control of relative orbital elements, and minimum separation distances.

Corollary results include that propellant savings are achieved by explicitly accounting for thruster configuration in the station-keeping strategy. It is shown that the classical sun-pointing perigee strategy is not required for typical electric propulsion thruster configurations in order to save propellant. And lastly it is shown that the thruster configuration itself has an impact on the orbit prediction and control accuracy.

II. Modeling of Equations of Motion

A. Review of Dynamics

The theory described in this section builds on foundations from [9]. A short review of the key concepts is given here. A linear time-varying formulation of the dynamics of a satellite in a geostationary orbit is obtained through two simplifying assumptions:

Assumption 1 *The input matrix at the ideal GEO-slot center provides a good approximation of the input matrix at an arbitrary position inside the GEO-slot.*

A similar assumption is applied to the perturbing accelerations:

Assumption 2 *The differential accelerations (excluding controlled accelerations) between a satellite at an arbitrary position inside a GEO-slot and a virtual satellite located at the GEO-slot center are at all times small.*

These assumptions were investigated in [9] and bounds on the maximum error resulting from these assumptions were given. The assumptions allowed to write the dynamics of a geostationary satellite as a linear time-varying system:

$$\dot{\mathbf{x}}(t) \approx \mathbf{A}\mathbf{x}(t) + \mathbf{B}(\alpha)\,\mathbf{u}_c(t) + \mathbf{B}(\alpha)\,\mathbf{u}_d(\mathbf{x}_{\text{geo}})\,. \tag{1}$$

The state is defined in the orbital element set introduced in [10] and is as follows:

$$\mathbf{x}(t) = \begin{pmatrix} \Delta n \\ e_y \\ e_x \\ i_y \\ i_x \\ \Delta L \end{pmatrix} = \begin{pmatrix} n - n_E \\ e\sin(\tilde{\omega}) \\ e\cos(\tilde{\omega}) \\ \sin\left(\frac{i}{2}\right)\sin(\Omega) \\ \sin\left(\frac{i}{2}\right)\cos(\Omega) \\ \varepsilon + \int_{t_0}^{t} n\mathrm{d}t - \alpha \end{pmatrix}, \tag{2}$$

where $n = \sqrt{\mu/a^3}$ is the mean orbital motion, n_E is the Earth's rotation rate, $\tilde{\omega} = \omega + \Omega$, ε is the mean longitude at epoch t_0, α is the right ascension of the geostationary position and a, e, i, ω, Ω are classical orbital elements. The $\mathbf{A}$ matrix contains all zeros, except the $(6,1)^{\text{th}}$-entry, which is equal to one. The input matrix $\mathbf{B}$ is evaluated at the geostationary slot center:

$$\mathbf{B}(\alpha) \approx \begin{pmatrix} 0 & \frac{-3}{a_{\text{GEO}}} & 0 \\ -\frac{1}{V_{\text{GEO}}}\cos\alpha & \frac{2}{V_{\text{GEO}}}\sin\alpha & 0 \\ \frac{1}{V_{\text{GEO}}}\sin\alpha & \frac{2}{V_{\text{GEO}}}\cos\alpha & 0 \\ 0 & 0 & \frac{1}{2V_{\text{GEO}}}\sin\alpha \\ 0 & 0 & \frac{1}{2V_{\text{GEO}}}\cos\alpha \\ -\frac{2}{V_{\text{GEO}}} & 0 & 0 \end{pmatrix}, \tag{3}$$

where V_{GEO} and a_{GEO} are respectively velocity and semi-major axis of an ideal geostationary orbit and the right ascension of the slot center is determined from:

$$\alpha(t) = \alpha(t_0) + n_E(t - t_0), \tag{4}$$

The perturbing accelerations $\mathbf{u}_d(\mathbf{x}_{\text{geo}})$ are determined at the slot center ($\mathbf{x}_{\text{GEO}}$) and both perturbing and controlled accelerations $\mathbf{u}_c(t)$ are defined in a radial, tangential, normal (RTN) reference frame.

In summary, the dynamics of a satellite relative to the geostationary slot center can be described by a linear time-varying system, driven by a perturbing acceleration $\mathbf{u}_d(t)$. References for obtaining an expression for the perturbing accelerations are ample, see e.g. [11], Chap. 3 or [12], Chap. 11 and 12. Both the perturbing acceleration and the time-varying input matrix $\mathbf{B}(t)$ are, for a given geostationary slot, non-linear but known function of time (under Assumptions 1 and 2).

B. Discretization of Dynamics

Equation (1) is discretized using a zero-order hold on the control input $\mathbf{u}_c(t)$, while applying the classic fourth-order Runge-Kutta (RK4) scheme to obtain the discrete update:

$$\mathbf{x}_{k+1} = \tilde{\mathbf{A}}\mathbf{x}_k + \tilde{\mathbf{B}}_k\mathbf{u}_k + \tilde{\mathbf{d}}_k, \tag{5}$$

where k refers to the k^{th} discrete step, $\tilde{\mathbf{A}}$, $\tilde{\mathbf{B}}_k$ and $\tilde{\mathbf{d}}_k$ are obtained by applying RK4 method to Eq. (1) for a certain timestep h. Note that $\mathbf{u}_k$ are the controlled accelerations and $\tilde{\mathbf{d}}_k$ contains the effect of perturbing accelerations. An explicit definition of the matrices is given in [9].

If we now repeatedly apply Eq. (5) from $k = 0$ to $k = N - 1$, we obtain the linear equation

$$X = \mathbf{F}\mathbf{x}_0 + \mathbf{H}U + \mathbf{J}D, \tag{6}$$

that relates the (concatenated) N future states $X = \left(\mathbf{x}_1^T, \mathbf{x}_2^T, ..., \mathbf{x}_N^T\right)^T$ to the current state $\mathbf{x}_0$ and the (concatenated) controls $U = \left(\mathbf{u}_0^T, \mathbf{u}_1^T, ..., \mathbf{u}_{N-1}^T\right)^T$. Disturbances $D = \left(\tilde{\mathbf{d}}_0^T, \tilde{\mathbf{d}}_1^T, ..., \tilde{\mathbf{d}}_{N-1}^T\right)^T$ and matrices $\mathbf{F}$, $\mathbf{H}$ and $\mathbf{J}$ follow from a repeated application of Eq. (5).

The development of this approach is extensively treated in [9] and explicit definitions of matrices are given there. The key feature of this formulation of the dynamics is that it provides an affine expression relating the osculating future states to the osculating current state and future controls, without neglecting the perturbing accelerations. It is this particular feature that enables us to solve problems of station-keeping and collocation using convex optimization techniques.

C. Thruster Configuration

Most common geostationary satellite are three-axis stabilized platforms with an Earth-pointing payload and solar panels on drive mechanisms. This design allows to keep the satellite attitude constant in an Earth-fixed reference frame and thus for a geostationary satellite also in the RTN reference frame. We state the assumption explicitly:

Assumption 3 *The satellite attitude is constant in the radial, tangential, normal reference frame*

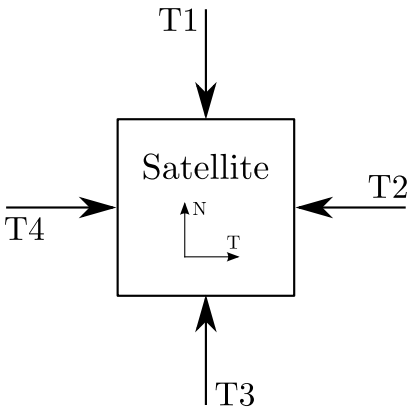

Fig. 1 Schematic of thruster configuration REF, none of the thrust vectors have a radial component.

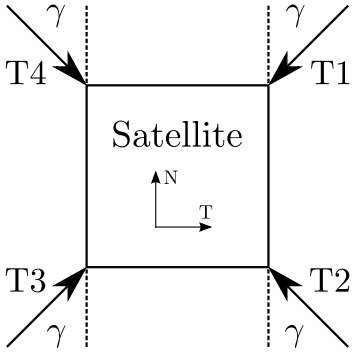

Fig. 2 Schematic of thruster configuration A, none of the thrust vectors have a radial component.

This assumption allows us to ignore attitude control in the station-keeping algorithm. Chemical propulsion thrusters are generally aligned with North, East, South and West directions, see the REF thruster configuration in Fig. 1. Such a thruster configuration ties in well with the dynamics, since the controlled accelerations are defined in radial, tangential and normal direction of the orbital reference frame (n.b. tangential and normal direction correspond to respectively East/West and North/South directions).

Satellites employing an electric propulsion system usually have a different layout. North and South sides are home to solar panels, and the plumes originating from an electric thruster can cause significant degradation of the solar panel. Hence, the thrusters are generally tilted away from the North and South directions to avoid contamination. We define two exemplary thruster

configuration with four thrusters. We seek symmetric configurations and describe the orientation of the thrusters by two rotations. For thrusters T1 and T4 we first rotate a vector pointing North over an angle $\gamma \in [0, 90°]$, while for T2 and T3 we rotate a vector pointing South over an angle $\gamma \in [0, 90°]$, both rotations are toward the radial direction. A second rotation is applied as follows; thrusters T1 and T2 are rotated by an angle $\beta \in [0, 90°]$ about the North-axis (towards the East) and T3 and T4 at an angle $\beta \in [0, 90°]$ about the South-axis (towards the West). One configuration (A) used in this paper is obtained for $\gamma = 45°$ and $\beta = 90°$, shown in Fig. 2. The arrows point in the direction of the acceleration that is exerted on the spacecraft by each thruster (which is opposite to the exhaust plume). With this choice for β and γ the thrust vector lies completely in the tangential, normal plane, which is a common choice for geostationary satellites. This configuration is similar as implemented on the Hispasat Advanced Generation 1 mission [13]. Another configuration (B) that is analyzed in this paper is obtained by choosing $\gamma = 45°$ and $\beta = 10°$,. Fig. 3 shows the projected thrust force vectors in the TN, RT and RN planes. Note that for this configuration the thrusters are all pointing away from the solar panels as well as away from the Earth-facing panel. We also use a reference configuration (REF) with four thrusters pointing respectively North, East, South and West (Fig. 1). Note that additionally the location of the thruster could be optimized, for example to support a combined orbit control and attitude control or momentum management strategy. The configurations used in this work assume each thrust force vector to pass through the satellite's center of mass and attitude dynamics are ignored.

For thruster configuration A, we could determine maneuvers in East/West and North/South directions and realize these maneuvers using the thrusters (e.g. a pure North maneuver would be executed by firing thrusters T2 and T3 simultaneously. Alternatively, the thruster configuration can be taken into account in the dynamics formulation by employing a matrix that maps the individual thrust directions to accelerations in the radial, tangential, normal plane. The second approach is used in this paper for two reasons: 1. it enables thruster configurations that cannot realize for instance, pure North or South maneuvers, such as configuration B, and 2. a slight reduction in propellant consumption is possible by directly optimizing the individual thruster firings. Thrust

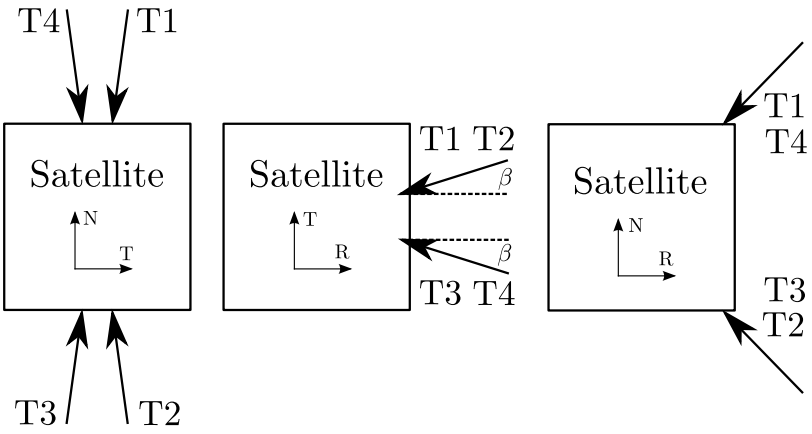

Fig. 3 Schematic of thruster configuration B with thrust vector projections on TN, RT and RN planes.

forces are mapped into radial, tangential, normal direction as follows;

$$\mathbf{u} = \frac{1}{m}\Gamma\mathbf{T}, \tag{7}$$

where m is the satellite mass, $\mathbf{T} = (T_1, T_2, T_3, T_4)^T$ is the vector of individual thrust forces and Γ is the thruster configuration matrix. For our definition of β and γ we obtain:

$$\Gamma = \begin{pmatrix} -\sin\gamma\cos\beta & -\sin\gamma\cos\beta & -\sin\gamma\cos\beta & -\sin\gamma\cos\beta \\ -\sin\gamma\sin\beta & -\sin\gamma\sin\beta & \sin\gamma\sin\beta & \sin\gamma\sin\beta \\ -\cos\gamma & \cos\gamma & \cos\gamma & -\cos\gamma \end{pmatrix} \tag{8}$$

This matrix can be used to reformulate Eq. (6) to:

$$X = \mathbf{F}\mathbf{x}_0 + \frac{1}{m}\mathbf{H}\mathbf{\Gamma}T + \mathbf{J}D, \tag{9}$$

with

$$\mathbf{\Gamma} = \begin{pmatrix} \Gamma & & \\ & \Gamma & \\ & & \ddots \end{pmatrix}.$$

and $T = \left(\mathbf{T}_0^T, \mathbf{T}_1^T, ..., \mathbf{T}_{N-1}^T\right)^T$. This formulation relates directly the thrusts by each thruster to the satellite state, described in non-singular orbital elements.

D. Relative Orbital Elements and Separation Distances

In this section we present a mapping between orbital elements differences and coordinates in the radial, tangential and normal reference frame attached to the leader satellite (x, y, z). The relative orbital elements are obtained by subtracting the leader element from the follower element, and are indicated by the Δ-symbol. The absolute orbital elements in the equations below refer to the leader satellite. This first-order mapping is found in [14], where it was introduced as part of a relative motion model:

$$\begin{aligned} x &\approx -\tfrac{2}{3}\tfrac{a}{n}\Delta n - a\Delta e_x \cos L - a\Delta e_y \sin L \\ y &\approx a\Delta L + 2a\Delta e_x \sin L - 2a\Delta e_y \cos L \\ z &\approx 2a\Delta i_x \sin L - 2a\Delta i_y \cos L. \end{aligned} \tag{10}$$

This linear mapping between relative orbital elements and the relative Cartesian position in the radial, tangential, normal (RTN) reference frame is valid for near circular, near equatorial orbits. The mapping is still depending on the leader's state. If required, this dependency can be removed by replacing a by a_{GEO}, n by n_{GEO} and L by α for satellites inside a geostationary slot (i.e. if the mapping is valid between two arbitrary satellites inside the slot, it is also valid between a satellite and its slot center).

We performed an error analysis of the linear mapping for the cases analyzed in the remainder of this paper and found that the relative error defined as:

$$e_{\mathrm{rel}} = \frac{\sqrt{e_x^2 + e_y^2 + e_z^2}}{\sqrt{x^2 + y^2 + z^2}}, \tag{11}$$

where e_x, e_y, e_z are the error between the approximate linear and exact nonlinear mapping, was at all times smaller than $1.4 \cdot 10^{-3}$. This statement is valid for the cases analyzed in this paper. Note that [6], Chap. 3.2, also introduces a mapping between relative orbital elements and relative separation distances for a slightly different orbital element set.

As done by d'Amico ([15], Chap. 2), we write relative eccentricity and inclination vectors in polar notation:

$$\Delta\mathbf{e} = \begin{pmatrix} \Delta e_x \\ \Delta e_y \end{pmatrix} = \delta e \begin{pmatrix} \cos\delta\tilde{\omega} \\ \sin\delta\tilde{\omega} \end{pmatrix} \tag{12}$$

$$\Delta\mathbf{i} = \begin{pmatrix} \Delta i_x \\ \\ \Delta i_y \end{pmatrix} = \sin\frac{\delta i}{2} \begin{pmatrix} \cos\delta\Omega \\ \\ \sin\delta\Omega \end{pmatrix} \approx \frac{\delta i}{2} \begin{pmatrix} \cos\delta\Omega \\ \\ \sin\delta\Omega \end{pmatrix}. \tag{13}$$

Note that we used respectively $\delta e \neq \Delta e$ and $\delta i \neq \Delta i$ to indicate the magnitude and $\delta\tilde{\omega} \neq \Delta\tilde{\omega}$ and $\delta\Omega \neq \Delta\Omega$ to indicate the phase of relative eccentricity and inclination vectors. Further defining $\delta M = L - \delta\tilde{\omega}$ as the angle between the satellite position the relative eccentricity vector and $\delta\omega = \delta\tilde{\omega} - \delta\Omega$ as the angle between relative eccentricity and inclination vectors allows to write the relative separation in RTN coordinates as:

$$\begin{aligned} x &\approx -\tfrac{2}{3}\tfrac{a}{n}\Delta n - a\delta e\cos\delta M \\ y &\approx a\Delta L + 2a\delta e\sin\delta M \\ z &\approx a\delta i\sin\left(\delta M + \delta\omega\right). \end{aligned} \tag{14}$$

These equations directly show the relation between the phasing of relative eccentricity and inclination vectors and corresponding relative motion. Note that $\delta\omega$ can be obtained directly from the relative eccentricity and inclination vectors:

$$\delta\omega = \cos^{-1}\left(\frac{(\Delta\mathbf{e})^T(\Delta\mathbf{i})}{\delta e\cdot\delta i}\right) \tag{15}$$

Due to the larger uncertainty in tangential direction, it is customary to rely on a separation distance in the radial-normal plane only. From Eq. (14) it can be observed that parallel relative eccentricity and inclination vectors (i.e. $\delta\omega = 0$ or $\delta\omega = 180°$) results in the largest separation in this plane, namely

$$\rho_{xz,\min} = \min\left(a\delta e, a\delta i\right). \tag{16}$$

Since in reality the satellites cannot be controlled to maintain $\delta\omega = 0$ at all times, we investigate the minimum separation distance in the radial-normal plane as a function of the relative eccentricity and inclination vectors. Assuming that the semi-major axis difference is small ($\Delta n \approx 0$), we have:

$$\rho_{xz}^2 = x^2 + z^2 = a^2\delta e^2\cos^2\delta M + a^2\delta i^2\sin^2\left(\delta M - \delta\omega\right) \tag{17}$$

with $\delta M \in [-\pi, \pi]$. For a particular configuration of relative eccentricity and inclination vectors, the minimum separation in the radial-normal plane can be found by minimizing Eq. (17) over δM,

as demonstrated below. We take the derivative of Eq. (17):

$$\frac{\mathrm{d}}{\mathrm{d}\delta M}\left(\rho_{xz}^2\right) = -a^2\delta e^2 \sin 2\delta M + a^2\delta i^2 \sin\left(2\delta M + 2\delta\omega\right) \tag{18}$$

which can be rewritten to

$$\frac{\mathrm{d}}{\mathrm{d}\delta M}\left(\rho_{xz}^2\right) = c_1 \sin\left(2\delta M + c_2\right), \tag{19}$$

where c_1 and c_2 are determined as follows:

$$c_1 = a^2\sqrt{\delta e^4 + \delta i^4 - 2\delta e^2\delta i^2 \cos 2\delta\omega} \tag{20}$$

$$c_2 = \mathrm{atan2}\left(\delta i^2 \sin 2\delta\omega,\ -\delta e^2 + \delta i^2 \cos 2\delta\omega\right). \tag{21}$$

The minimum is found by solving

$$\frac{\mathrm{d}}{\mathrm{d}\delta M}\left(\rho_{xz}^2\right) = 0, \tag{22}$$

which occurs at $\delta M = -c_2/2 + k/2\cdot\pi$, and hence there are four solutions in the domain of interest, two corresponding to the maximum separation distance, and two corresponding to the minimum separation distance. The symmetry of the relative motion requires us to only examine one of the two solutions to find the minimum distance. If we choose $\delta M = -c_2/2$ we can verify ($c_1 > 0$):

$$\frac{\mathrm{d}^2}{\mathrm{d}\delta M^2}\left(\rho_{xz}^2\right) = 2c_1 \cos\left(2\delta M + c_2\right) > 0, \tag{23}$$

and hence the minimum is obtained. The minimum is found by substituting $\delta M = -c_2/2$ in Eq. (17) and taking the square root:

$$\rho_{xz,\min} = a\sqrt{\delta e^2 \cos^2\left(-\frac{c_2}{2}\right) + \delta i^2 \sin^2\left(-\frac{c_2}{2} - \delta\omega\right)}. \tag{24}$$

This equation can be used to find the minimum separation distance as a function of the relative eccentricity and inclination vectors.

E. Safe Separation Strategy

We use a leader/follower architecture for controlling a fleet of collocated satellites. One designated leader satellite is controlled using some desired approach and it is assumed that the predicted

leader state trajectory $\mathbf{x}^L(t)$ is available to each follower satellite (n.b to obtain a "predicted" state, the current state is propagated using the latest maneuver plan). The follower satellites are controlled relative to this leader trajectory and are generally assumed to follow this trajectory to within predefined control windows that are different for each follower.

The typical coordination strategy for collocated geostationary satellites is the eccentricity-inclination vector separation strategy ([2], [16]). This strategy relies fully on the radial-normal plane to ensure safe separation. The key idea behind this strategy is to control the relative eccentricity and inclination vectors such that radial and normal motion are approximately 90° out-of-phase and thus, normal separation is maximal when radial separation vanishes and vice-versa. As discussed in the previous section, this situation occurs when relative eccentricity and inclination vectors are parallel (i.e. $\delta\omega = 0$).

We adopt this strategy and define nominal relative e/i-vectors between follower and leader satellites so that $\delta e = \delta i$ and $\delta\omega = 0$. The relative eccentricity and inclination vectors are then controlled within tolerance windows, centered on the nominal relative e/i-vectors and bounded by the $\ell 2$-norm:

$$\Delta\mathbf{e} \in S_e\left(\Delta\mathbf{e}_c, r_e\right) = \left\{\Delta\mathbf{e} \mid \left\|\Delta\mathbf{e} - \Delta\mathbf{e}_c\right\|_2 \leq r_e\right\} \tag{25}$$

$$\Delta\mathbf{i} \in S_i\left(\Delta\mathbf{i}_c, r_i\right) = \left\{\Delta\mathbf{i} \mid \left\|\Delta\mathbf{i} - \Delta\mathbf{i}_c\right\|_2 \leq r_i\right\}, \tag{26}$$

where $\Delta\mathbf{e}_c$ and $\Delta\mathbf{i}_c$ are respectively the nominal relative eccentricity and inclination vectors and r_e and r_i are the corresponding bounds. An exemplary configuration used in this paper, including tolerance windows, can be seen in Figs. 5 and 6.

The key question is; what is the minimum separation distance for relative eccentricity and inclination vectors inside these (convex) tolerance windows? From the equations presented before we can deduce that the minimum separation distance decreases for increasing $\delta\omega$ and decreasing δe and δi. The control windows are defined for relative orbital elements between follower and leader satellites. If two follower satellites' relative e/i vectors are controlled within these windows, these two follower satellites can have larger $\delta\omega$ and smaller δe and δi with respect to each other. Note that in these terms, the worst case (in Figs. 5 and 6) occurs between F1 and F2, or equivalently between

F2 and F3 and an equivalent tolerance window is found by assuming F2 fixed and enlarging the tolerance window on F3 to $2r_e$ and $2r_i$. To find an exact bound on the smallest minimum separation distance we can solve the non-convex optimization problem

$$\begin{aligned} &\text{minimize} && \rho_{xz,\min} \\ &\text{subject to} && \\ & && \Delta\mathbf{e} \ \in \ S_e \\ & && \Delta\mathbf{i} \ \in \ S_i. \end{aligned} \tag{27}$$

If we set $\Delta\mathbf{e}_c = \Delta\mathbf{i}_c$ and $r_e = r_i$ and assume $\Delta\mathbf{e}^T\Delta\mathbf{i} > 0$ for all $\Delta\mathbf{e} \in S_e$ and $\Delta\mathbf{i} \in S_i$ (which is a very reasonable assumption, since $\Delta\mathbf{e}^T\Delta\mathbf{i} = 0$ would result in $\rho_{xz,\min} = 0$), we find an analytic solution to the optimization problem in Eq. (27) by substituting:

$$\delta e = \delta i = \sqrt{r_e^2 + \delta e_c^2 - \sqrt{2} r_e \delta e_c} \quad \text{and} \quad \delta\omega = \sqrt{2}\frac{r_e}{\delta e} \tag{28}$$

into Eq. (24). Note that we need to substitute $2r_e$ to find the minimum separation distance between two follower satellites. Thus by choosing a set of (convex) control windows on relative eccentricity and inclination vectors, and maintaining the relative orbital elements within these windows, we can guarantee a certain minimum separation distance, calculated either by solving Eq. (27) or under more restricted conditions from Eqs. (24) and (28).

This approach provides an alternative method to deal with the non-convex constraint of maintaining a minimum separation distance between satellites. The great advantage of this approach is that we are able to deal with the minimum separation distance constraint by defining two different convex constraints. Since these constraints are defined with respect to (relative) orbital elements, the satellites follow a very natural orbital motion (i.e. the (relative) orbital elements are integration *constants* in the Keplerian two-body problem). The only disturbances that require compensation are resulting from differential orbital perturbations, controlled accelerations from the leader satellite and disturbances resulting from sensor and actuator errors.

III. Collocation as a Convex Optimization Problem

In this section we will extend the approach introduced in [9] to a fleet of collocated satellites with constraints on relative states.

A. Relative State, State Error and Constraints

The relative state is obtained by subtracting the leader state from the follower state. The leader state $\mathbf{x}^L(t)$ is sampled at the discrete time points matching the discretized follower state to obtain X^L and the relative state is formed as follows:

$$\begin{aligned}\Delta X^i &= X^i - X^L \\ &= \mathbf{F}\mathbf{x}_0^i + \frac{1}{m^i}\mathbf{H}\mathbf{\Gamma}^i T^i + \mathbf{J}D^i - X^L,\end{aligned} \tag{29}$$

where $i = 1, 2, 3, ...$ refers to the i^{th} follower satellite. Note that also the term D is different for each satellite in the fleet, as it depends on all dominant perturbations, including solar radiation pressure, which in turn is dependent on the particular satellite's characteristics. Actually, differential perturbations other than solar radiation pressure are very similar for the different satellites, and could be canceled in forming the relative state. We however decided to maintain also these perturbations, as it allows us to evaluate also the absolute state and possibly constrain it. Now let ΔX^i_{des} be the desired relative state of follower satellite i, the state error is then defined as:

$$\begin{aligned}E^i &= \Delta X^i - \Delta X^i_{\text{des}} \\ &= \mathbf{F}\mathbf{x}_k^i + \frac{1}{m^i}\mathbf{H}\mathbf{\Gamma}^i T^i + \mathbf{J}D^i - X^L - \Delta X^i_{\text{des}},\end{aligned} \tag{30}$$

The key task of the collocation control algorithm is to maintain a convex function of this error below a certain bound

$$C^i\left(E^i\right) \leq C^i_{\text{ub}}, \tag{31}$$

or an affine function of this error between an upper an a lower bound

$$C^i_{\text{lb}} \leq C^i\left(E^i\right) \leq C^i_{\text{ub}}, \tag{32}$$

where $C^i\left(E^i\right)$ are state constraint functions, "lb" and "ub" refer to respectively lower and upper bounds.

B. Scaling of the State and Control Variables

In the formulation of an optimization problem it is good practice to scale optimization variables and constraints so that they vary in more uniform ranges. Proper scaling enhances robustness and

improves converges of the optimization problem [17]. The optimization variables (i.e. thrust) are scaled so that they vary in the range $[0, 1]$, which is achieved by applying the following scaling law:

$$\begin{aligned}\bar{\mathbf{T}}^i &= \mathcal{T}^i \mathbf{T}^i \\ &= \begin{pmatrix} 1/T^i_{1,\max} & & & \\ & 1/T^i_{2,\max} & & \\ & & 1/T^i_{3,\max} & \\ & & & 1/T^i_{4,\max} \end{pmatrix} \mathbf{T}^i,\end{aligned} \tag{33}$$

where $T_{\max}$ denotes the (maximum) thrust that a particular thruster can deliver. The complete (concatenated) vector of thrusts in the range $k = 1, .., N$ is defined as:

$$\begin{aligned}\bar{T}^i &= \boldsymbol{\mathcal{T}}^i T^i \\ &= \begin{pmatrix} \mathcal{T}^i & & \\ & \mathcal{T}^i & \\ & & \ddots \end{pmatrix} T^i.\end{aligned} \tag{34}$$

A similar approach is applied to the constraints. In this work we only consider affine constraints that have symmetric bounds (i.e. $C^i_{\text{lb}} = -C^i_{\text{ub}}$) or convex constraints which are greater than or equal to zero, with only an upper bound. If c^i_j denotes the j^{th} element of C^i, we scale that constraint by $1/c^i_{j,\text{ub}}$, so that the scaled constraint $\bar{c}^i_j$ varies in the range $[0, 1]$ or $[-1, 1]$, for respectively $c^i_{j,\text{lb}} = 0$ and $c^i_{j,\text{lb}} = -c^i_{j,\text{ub}}$. Similar to the thrust vector scaling, we define a diagonal scaling matrix for the constraints:

$$\begin{aligned}\bar{C}^i &= \boldsymbol{\mathcal{C}}^i C^i \\ &= \begin{pmatrix} 1/c^i_{j,\text{ub}} & & \\ & 1/c^i_{j,\text{ub}} & \\ & & \ddots \end{pmatrix} C^i.\end{aligned} \tag{35}$$

These scaled variables are used in the formulation of the optimization problem in the next section.

C. Optimization Problem Formulation

An optimization based method is used to determine the station-keeping maneuvers of the follower satellites. This section details the formulation of the optimization problem. To solve the

collocation control problem for follower satellite i we specify the following optimization problem:

$$\begin{aligned} \text{minimize} \quad & \alpha\|\bar{T}^i\|_1 + (1-\alpha)\sum_{j=1}^{M}\max\left(0, s_j - 1\right) \\ \text{subject to} \quad & \\ & \bar{C}^i \;\leq\; \mathbf{s} \\ & \bar{T}^i \;\geq\; \mathbf{0} \\ & \bar{T}^i \;\leq\; \mathbf{1}. \end{aligned} \tag{36}$$

The optimization variables in this problem are 1. the scaled thrust vector $\bar{T}^i$, and 2. a slack variable vector $\mathbf{s}$, which has length of M, equal to the number of constraints $\bar{C}^i$.

1. Cost Function

The cost function contains two terms, the first is the $\ell 1$-norm of the thrust vector. This term represents the minimization of propellant consumption. The second term is a deadzone-linear penalty function [18], which can be interpreted as follows; whenever the slack variable s_j is smaller (in absolute terms) than the tolerable bound on the constraint function $c^i_{j,\text{ub}}$, it is free of charge. Whenever the bound gets violated, it is penalized through the cost function. This implementation gives the optimizer an option to violate desired control windows on state variables at a cost. The advantage of this implementation is that the optimization problem does not become infeasible when the constraints cannot be met. A relative weighting between the two terms in the cost function is added through α (with $\alpha \in [0, 1]$). A further weighting on the slack variables can be included to distinguish their relative importance.

2. Constraints

Three types of state constraints were used in this work. The first two constraint types are bounds on the $\ell 2$-norm of the eccentricity and inclination vector error $(\Delta e_x, \Delta e_y)^T$ and $(\Delta i_x, \Delta i_y)^T$. To arrive at a specific example, let $E^i_{j,k}$ denote the j^{th} relative state error at discrete time k. A constraint on the $\ell 2$-norm of the eccentricity vector error at time k, including scaling and slack variable is as follows:

$$\frac{1}{c^i_{j,\mathrm{ub}}} \left\| \begin{matrix} E^i_{2,k} \\ E^i_{3,k} \end{matrix} \right\|_2 \leq s_j \tag{37}$$

and on the inclination vector error:

$$\frac{1}{c^i_{j,\mathrm{ub}}} \left\| \begin{matrix} E^i_{4,k} \\ E^i_{5,k} \end{matrix} \right\|_2 \leq s_j. \tag{38}$$

The third type of constraint is a box constraint on the longitude error ΔL, implemented as:

$$\frac{1}{c^i_{j,\mathrm{ub}}} \left| E^i_{6,k} \right| \leq s_j. \tag{39}$$

The constraint on the control variables $\bar{T}$ are bounds on the maximum thrust force that the satellite can deliver. After applying the scaling, each element in $\bar{T}$ is bounded between 0 and 1.

D. Implementation of Maneuver Plans

The maneuver plans resulting from solving the optimization problem in Eq. (36) are processed before they are implemented. This is required because we assume that the thrusters have only a single qualified operational point and are hence on/off thrusters. Since we penalize the $\ell 1$-norm of the thrust vector in the cost function, the resulting maneuver plans are always sparse (i.e. they contain only a small number of non-zero elements). In realizing the maneuver plans we use the following logic; if subsequent time intervals for a single thruster have a non-zero thrust, these are combined into a single burn, centered on a weighted average of the individual thrusts, with a magnitude equal to $T_{\max}$, and a duration such that the total impulse is equal to the sum of the individual elements. This process is visualized in Fig. 4. No more than three subsequent intervals are combined into a single burn so that the error resulting from this processing remains bounded. A short analysis on the magnitude of the error thus introduced is presented in [9] and is more than an order of magnitude smaller than errors resulting from e.g. orbit determination or the thrusters themselves.

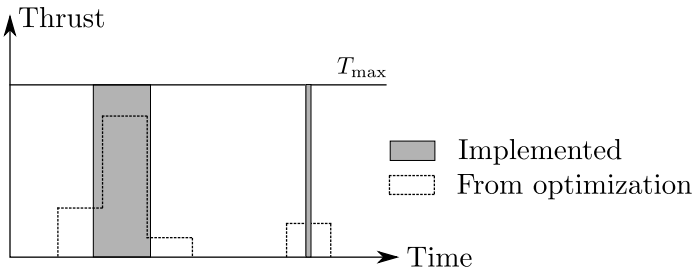

Fig. 4 Conceptual sketch showing the implementation of a maneuver plan resulting from optimization.

IV. Simulation and Analysis

This section presents the simulation environment and two analysis cases to evaluate the presented method for controlling collocated satellites.

A. Simulation Environment

Simulations were carried out using Matlab. We used a validated propagator including Earth gravity up to 8^{th} order and degree, Moon gravity, Sun gravity and solar radiation pressure (SRP). The RK4 integration method was used, with a timestep of 100 seconds. The optimization problem was formulated using CVX [19], and solved using MOSEK [20]. The timestep in the optimization problem was 1000 s, so that 87 steps are needed for to completely cover one orbit. Maneuver plans were implemented based on simple on/off thruster with a single operational point (i.e. $T = 0$ or $T = T_{\max}$). The thrusters are assumed to have a minimum on-time as well, to avoid large uncertainty in the thrust force due to the transient behavior at switch-on and switch-off. Several forms of uncertainty were included; Gaussian orbit determination errors were implemented based on the covariance matrix in Table 1, actuator uncertainty was included by implementing a 5% thrust force error (Gaussian, 3σ) and a 1.5° attitude error (Gaussian, 3σ). In addition, SRP uncertainty was included as a 15% uniform random error on the acceleration due to SRP.

B. Analysis Cases

We present two concrete example cases of a fleet of satellites controlled in geostationary slots of respectively ±0.1° and ±0.05°, located at 19.2°E. In the first case, the leader satellite is controlled

Table 1 Covariance matrix of orbit determination error, Radial (R), Tangential (T) and Normal (N) position [m^2] and velocity (V) [m^2/s^2]

	R	T	N	VR	VT	VN
R	1.23E+01	4.90E+01	1.12E+01	2.95E−04	-1.70E−03	-1.94E−03
T	4.90E+01	1.47E+05	-1.56E+02	2.09E−03	-7.86E−03	2.74E−02
N	1.12E+01	-1.56E+02	1.32E+02	2.31E−04	-1.50E−03	-2.30E−02
VR	2.95E−04	2.09E−03	2.31E−04	9.20E−09	-4.33E−08	-4.02E−08
VT	-1.70E−03	-7.86E−03	-1.50E−03	-4.33E−08	2.37E−07	2.61E−07
VN	-1.94E−03	2.74E−02	-2.30E−02	-4.02E−08	2.61E−07	4.00E−06

using a sun-pointing perigee strategy, while in the second case the mean eccentricity is controlled to a fixed point. The leader's inclination control strategy is such that only secular variations of the inclination vector are compensated, while the periodic oscillations are uncontrolled. The longitude control strategy targets the center of the slot at the end of the maneuver cycle in both cases. More specifically, the leader satellite was controlled using the method outlined in [9], without constraints on the thrust other than the maximum thrust force. The predicted leader state trajectory was made available to the follower satellites. The follower satellites are then controlled relative to the leader satellite using the method outlined in the previous section.

1. Case A: a Fleet of Four Satellites

With this simulation case we aim to show that the method is robust under realistic (/conservative) assumptions on uncertainty, for a maneuver cycle of 7 days (in line with typical maneuver cycle durations for electric propulsion spacecraft see e.g. [21]), for a fleet of satellite with differences in mass, surface area and propulsion system. We aim to show that the method has no significant penalties in performance, while maintaining safe separation distances. Performance is measured in terms of propellant consumption and number of thruster firings.

The fleet consists of four satellites. The follower satellites have characteristics different from the leader satellite in terms of area exposed to the Sun, maximum thrust force and minimum impulse bit. Between the three follower satellites the characteristics are identical, with the exception of

their thruster configuration. The satellite characteristics are summarized in Table 2. The maneuver plans for the follower satellites are determined with a prediction horizon of 7 days, in line with usual operational practice, which are then executed open-loop. The leader follows a Sun-pointing perigee strategy, following a circle in the eccentricity plane with a radius of $2{\cdot}10^{-4}$, the eccentricity circle's center and other nominal leader parameters are given in Table 3.

Table 4 shows the bounds that were implemented in the optimization problem. Figures 5 and 6 show the eccentricity and inclination vector configuration. The nominal relative states of the follower satellites were chosen consistent with the e/i vector separation strategy. The dashed line shows the bounds in the optimization problem. The absolute worst-case minimum separation distance (in the radial-normal plane) can be found by solving Eq. (27) (using the analytical solution from Eq. (28)) and using a bound of $2r_e$ (which would be the maximum bound between two follower satellites' relative eccentricity and inclination control windows). The resulting worst-case minimum separation distance in the radial-normal plane is found to be:

$$\rho_{xz,\min} \geq 6.03 \text{ km} \tag{40}$$

which occurs at $\gamma = 36.24°$, with $\delta e = \delta i = 2.24 \cdot 10^{-4}$. Thus maintaining the relative eccentricity and inclination vectors within the specified convex bounds guarantees the above stated minimum separation distance.

Note that due to the implementation of the constraints with slack variables $\mathbf{s}$, which are penalized using a deadzone linear term in the cost function in Eq. (36) the constraints are not hard bounds, instead, they could be violated, such that the resulting optimization problem is always feasible. We found that especially in the presence of errors (orbit determination, actuators, modeling) performance increased when we implemented a tighter bound on the final state. We also found that it is good practice to make the satellite with the least capable propulsion system, in terms of maximum acceleration of the spacecraft, the formation leader. The underlying reason is that a formation leader with a significantly more capable propulsion system could produce reference trajectories which cannot be realized by satellite with a less capable propulsion system.

Table 2 Parameters of four satellites

Parameter	L	1	2	3
Mass [kg]	3000	3000	3000	3000
Surface area [m^2]	90	120	120	120
Reflection coefficient [-]	1.2	1.2	1.2	1.2
Thrust force [mN]	75	125	125	125
Minimum on-time [s]	60	60	60	60
Thruster configuration	REF	REF	A	B

Table 3 Leader nominal mean orbital elements

	Case A	Case B
e_x [-]	-1.41E-04	-0.60E-04
e_y [-]	1.41E-04	0.60E-04
i_x [rad]	-0.71E-04	-0.30E-04
i_y [rad]	0.71E-04	0.30E-04
ΔL [rad]	0	0

2. Case B: a Fleet of 16 Satellites

If we desire to control the relative orbital elements within tighter bounds, under the assumed errors in orbit determination, actuation and modeling, we can only do so by increasing the frequency of re-planning. To avoid unnecessary burden on the operator, the method can and should be implemented in a fully automated manner. A necessary element to achieve autonomous station-keeping is an automated orbit determination capability, which can, e.g., be enabled by an on-board

Table 4 Bounds on different state constraints

	Case A		Case B	
$c^i_{j,\mathrm{ub}}$	at $k<N$	at $k=N$	at $k<N$	at $k=N$
r_e [-]	5.00E-05	2.50E-05	2.50E-05	1.25E-05
r_i [rad]	5.00E-05	2.50E-05	2.50E-05	1.25E-05
ΔL [rad]	2.00E-04	5.00E-05	1.00E-04	5.00E-05

GNSS receiver, see e.g [22], containing acceptance testing performance results for a GPS receiver in GEO. Their results are significantly better than the orbit determination uncertainty assumed in this work. Assuming such capability, we investigated the collocation of a fleet of 16 satellites in a $\pm 0.5^\circ$ slot, using the proposed method. The leader's nominal mean orbital elements are given in Table 3. The nominal inclination and eccentricity vector configuration can be easily derived from Fig.9 and Fig. 10. In this case we assumed identical satellites, with thruster configuration B. The satellite characteristics are identical to follower 3 in case A (see Table 2). Making a similar analysis as in case A, we can guarantee minimum separation distances in the radial-normal plane larger than 2.13 km. We further aim to maintain performance in terms of propellant consumption and number of maneuvers, despite of the much shorter maneuver cycle. Note that this case significantly improves the state-of-art as currently up to 8 satellites have been collocated in a slot that is twice the size in longitude ($\pm 0.1^\circ$) and hence quadruple the size in the eccentricity / inclination plane.

Table 5 Propellant consumption and thruster firings for a time-span of one year, case A

	L	F1	F2	F3
ΔV [m/s]	49.86	50.87	68.10	68.06
Pulses	900	901	1458	1361

V. Results and Discussion

A. Case A

Figures 5 to 7 show the results of case A for respectively relative eccentricity control, relative inclination control and relative mean longitude control. The dashed lines indicate the soft constraints as formulated in the optimization problem. Table 5 contains results in terms of propellant consumption (measured in ΔV) and number of thruster firings. Figure 8 shows an exemplary maneuver plan for a period of one week, for the third follower satellite.

A geostationary satellite with a low thrust propulsion system usually requires usually one or two North-South and one or two East-West maneuvers per day [21], which, depending on the thruster configuration, can be realized with two to eight burns per day. Hence, the expected number of burns for a satellite with a low-thrust electric propulsion system is between 730 and 2920 per year and

anything in this range is deemed acceptable. A lower bound on the required ΔV can be established by analyzing the drift of the mean inclination vector due to luni-solar perturbations over one year and calculating impulsive ΔV required to compensate this drift. This has been done for the simulation settings in this paper and the result is 47.8 m/s for the REF configuration. For configuration A and B this value has to be multiplied by $\sqrt{2}$ due to the cosine loss in the North/South direction, the resulting ΔV is equal to 67.6 m/s. Note that is an absolute lower bound and that these ΔV-values consider only North-South corrections. Another 2-3 m/s per year is to be expected for East-West station-keeping.

The results in terms of ΔV and number of firings in Table 5 are very much in line with expectations. We note that by explicitly taking the thruster configuration into account in the optimization problem, we saved 2-4 m/s ΔV for configuration A and B. Note that in case of configuration A, we could optimize for North-South and East-West burns and realize each burn by simultaneous firing of two thrusters. The resulting ΔV would then be approximately equal to that of Follower 1, multiplied by $\sqrt{2}$. We could not deal with configuration B at all without explicitly accounting for the thruster configuration as part of the optimization problem.

We observe that follower 1 required 1.0 m/s more ΔV than the leader satellite, despite of having the same thruster configuration. The main reason for this increase in propellant consumption is the higher solar radiation pressure on follower 1. We further observe that the satellites with thruster configurations A and B require more pulses than for the reference configuration. This result has the following explanation; most maneuvers are in North-South direction and each maneuver in North-South direction requires two thruster pulses for configuration A and B, whereas with the REF configuration a North or South maneuver is realized with a single thruster pulse. The exemplary thrust profile of F3 in Fig. 8 shows that the resulting maneuver plans are sparse, with only few thruster firings each day. We further see that thruster firings of T1 and T4 (South) and T2 and T3 (North) are often synchronized to achieve respectively South and North maneuvers.

We analyzed the minimum separation distance in the radial-normal plane, for every satellite pair (6 combinations). We found that the minimum separation distance in the radial, normal plane was equal to 8.82 km over the full one year simulation, which is much higher than the theoretical

minimum of 6.04 km. We also looked into the difference between the state trajectory resulting from the optimization, based on the linearized model in Eq. (6), and the state trajectory resulting from propagation (our "real" world). This difference includes the effects of the modeling errors, orbit determination errors, actuator errors and the processing of the maneuver plans. Table 6 presents the results in RTN reference frame. We evaluated both the mean error at the end of the maneuver cycle and the maximum error that occurred during the simulation.

An important observation from Table 6 is that the worst-case error in radial and normal direction is much smaller than the minimum separation distance, hence the current configuration is very conservative in terms of maintaining a minimum separation distance. In other words, we could design a configuration with a much smaller minimum separation distance without significantly increasing collision risk. Another important observation is the importance of the thruster configuration on the accuracy of orbit prediction and control. We observe that errors in radial and tangential direction are significantly degraded for thruster configuration A. The key reason for this behavior is that both thrust force errors and attitude errors for every firing can have significant components in East/West direction. Since both the eccentricity and longitude are very sensitive to East/West thrust errors, we observe large errors in radial and tangential direction. In configuration B this problem is much smaller, since the East-West component of thrust is very small, and hence, errors in the thrust force magnitude have almost no component in East-West direction. Errors in thrust force direction can still have a significant component in East-West direction.

In summary; a sufficient separation distance was achieved and the results in terms of propellant consumption and thruster firings were also very much within acceptable range. This simulation case considered a large slot, and large control windows for the relative orbital elements. To increase the number of satellites in the slot the satellites need to be controlled within tighter control windows. This could be achieved by reducing the maneuver cycle duration, which is demonstrated in case B.

B. Case B

Figures 9 and 10 show the results of case B. The results show only minor violations of the control windows (which were much smaller than the control windows in case A). We further analyzed

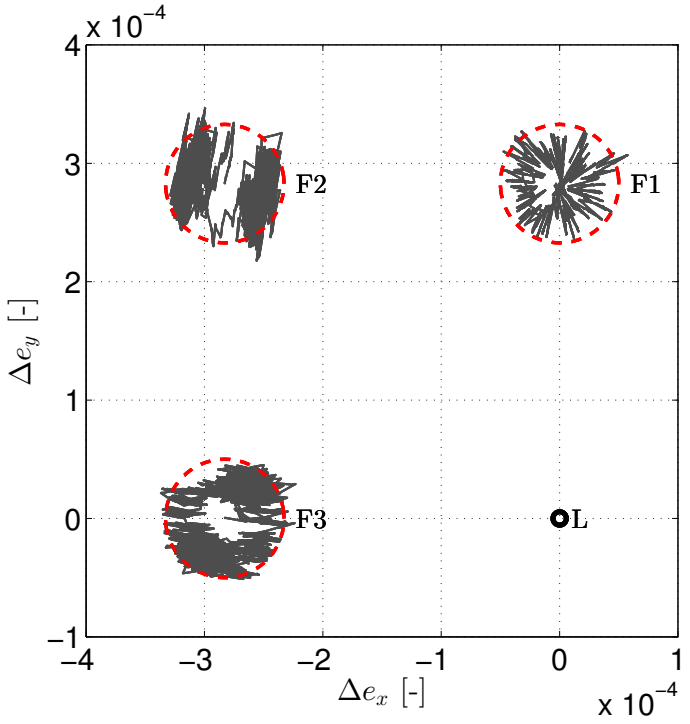

Fig. 5 Relative eccentricity vector, case A.

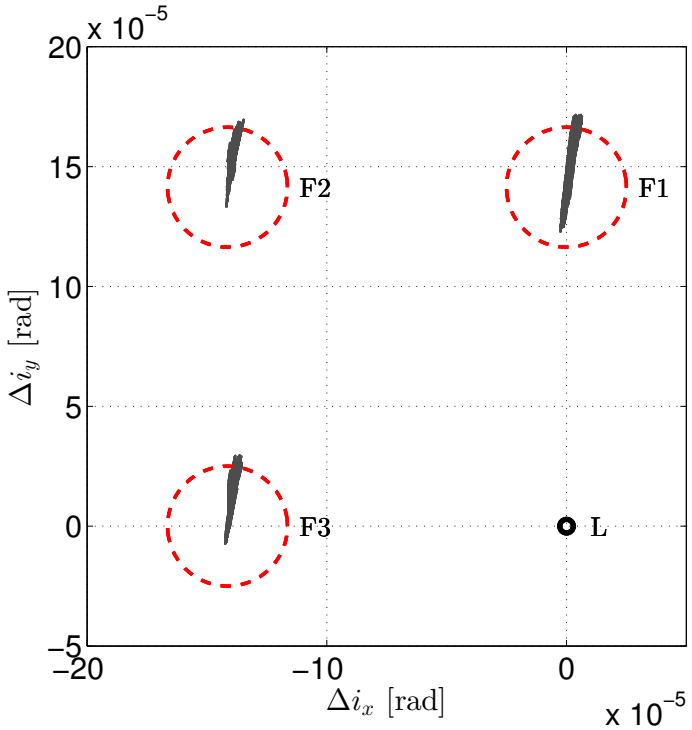

Fig. 6 Relative inclination vector, case A.

Table 6 Mean and maximum difference of the satellite position resulting from the solution of the optimization problem in comparison to the propagated satellite position at the end of a maneuver cycle, over a 1 year simulation, case A.

		L	F1	F2	F3
ΔR_{mean}	[km]	0.05	0.07	0.11	0.08
ΔT_{mean}	[km]	1.36	1.71	3.28	1.42
ΔN_{mean}	[km]	0.04	0.03	0.02	0.04
ΔR_{max}	[km]	0.30	0.45	0.62	0.49
ΔT_{max}	[km]	4.62	5.06	10.07	3.60
ΔN_{max}	[km]	0.19	0.20	0.15	0.13

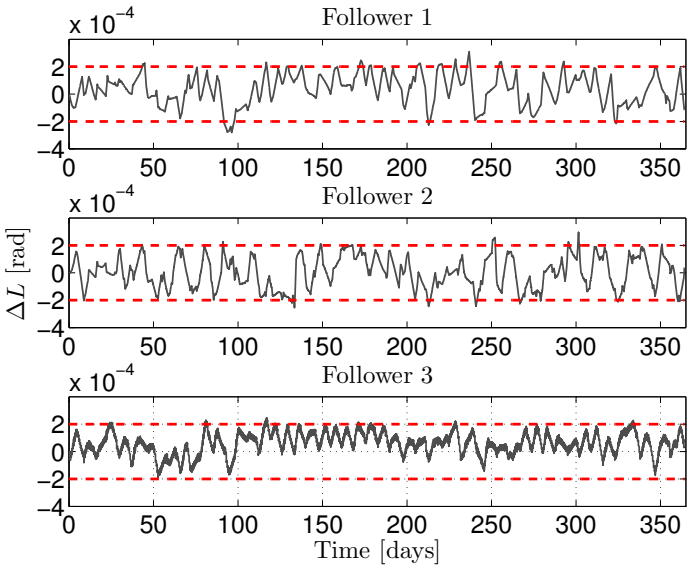

Fig. 7 Relative mean longitude, case A.

whether no satellite left the geostationary slot. We found that all satellites remained within the longitude window $[-0.048°,\ 0.047°]$. The worst-case minimum separation distance in the radial-normal plane among all 120 pairs was equal to 3.36 km, which is much better than the theoretically possible worst case of 2.13 km. This worst-case occurred between follower 10 and follower 11. The relative motion in the radial-normal plane between these two satellites is shown in Fig. 11.

We then looked into the difference between the trajectory as calculated by the optimizer and the trajectory actually flown (including effects of modeling errors, orbit determination errors and

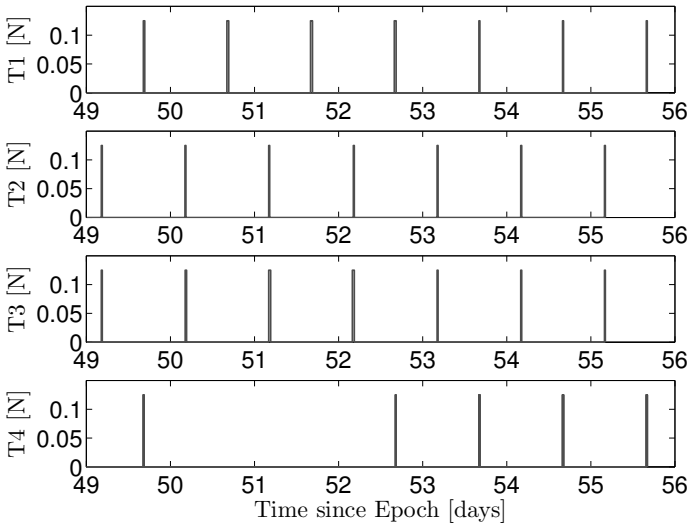

Fig. 8 Exemplary maneuver plan, 8^{th} week, case A.

actuator errors) and found the following maximum errors over the complete one year simulation, over all satellites of 153.9 m in Radial direction, 1739.3 m in Tangential direction and 81.6 m in Normal direction. These results further confirm that it is a good choice to ensure safe separation using only the radial-normal plane. The errors between predicted and actual trajectories are very acceptable and the combined radial, normal error is far smaller than the achieved minimum separation distances, allowing us to conclude that the strategy is safe, even with 16 satellites in a small geostationary slot. It shows that we could further reduce the minimum separation distance and allow an even greater number of satellites to be controlled safely within a single slot.

The average ΔV required for controlling the fleet was equal to 68.69 m/s and the average number of thruster pulses was equal to 1440 pulses. Only a minor increase in ΔV was observed compared to case A, even though no sun-pointing perigee was followed in case B. The minor increase is due to the more frequent calculation of maneuver plans, and hence, more frequent compensation of orbit determination errors. The reason that no Sun-pointing perigee strategy is required to save propellant is that the satellites require much more ΔV in N/S direction than in E/W direction and since the thrusters are inclined with respect to the N/S plane, every thruster firing for N/S control basically provides a "free" E/W thrust. By accounting for the thruster configuration in the optimization problem we were able to use this to our benefit. Thus for satellites with typical electric propulsion thruster configurations, a sun-pointing perigee strategy is not required to save

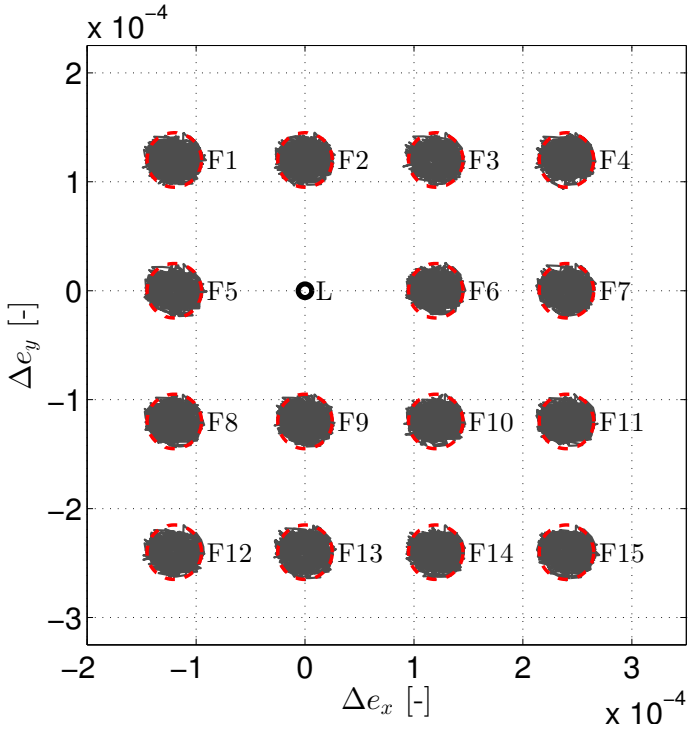

Fig. 9 Relative eccentricity vector, case B.

propellant, leaving more space in the eccentricity vector plane, and allowing to accommodate more satellites within a single slot.

VI. Conclusion

This paper presented a method for station-keeping of a fleet of satellites collocated in a geostationary slot. The maneuver plans were calculated based on relative orbital elements, while using convex optimization techniques in a leader-follower control hierarchy. The method was demonstrated to be propellant-efficient, requiring an acceptable number of maneuvers, while maintaining sufficiently large separation distances.

It was demonstrated that relative orbital elements are suitable for controlling the relative motion of a fleet of satellites in a geostationary orbit. The relative orbital elements provide a direct measure for relative separation distances and controlling relative eccentricity and inclination vectors in convex control windows guarantees a minimum separation distance in the radial normal plane. At the same time the bounds on the absolute orbital elements can guarantee that satellites remain inside the geostationary slot. Since orbital elements are integration constants in the Keplerian two-

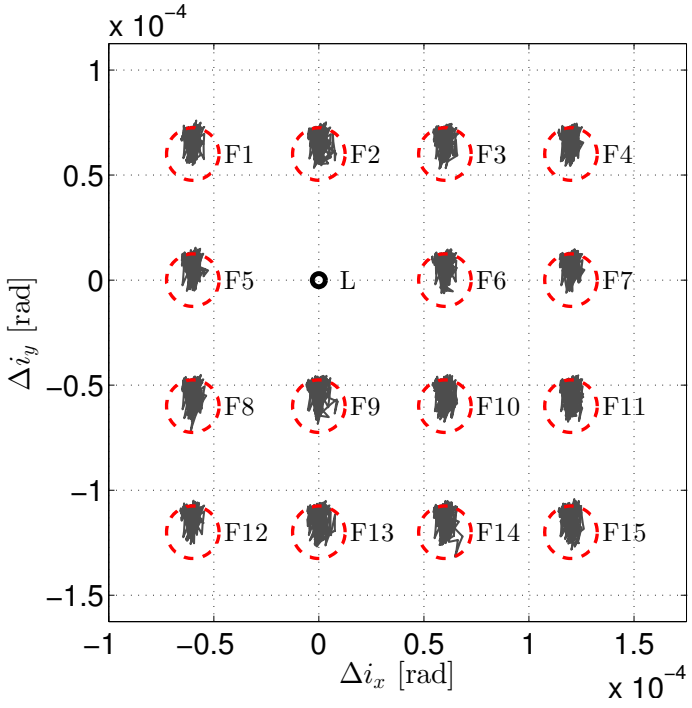

Fig. 10 Relative inclination vector, case B.

body problem, the resulting motion is a natural orbital motion.

The relative station-keeping problem was formulated as a convex optimization problem, which was achieved by using a linear time-varying formulation of the satellite dynamics. The optimization problem aimed at minimizing propellant consumption, while maintaining the relative states inside convex control windows. The particular formulation resulted in a sparse solution, with limited thruster firings, realizable by a simple on/off propulsion system.

The method was demonstrated to work for a fleet of satellites with different design characteristics, under realistic errors in orbit determination, actuation and modeling for maneuver cycles of one week. It was shown that significant advantages are obtained for shorter maneuver cycles and it was demonstrated that 16 satellites can be controlled in a $\pm 0.05^\circ$ longitude slot, while maintaining safe separation distances and with good performance in terms of thruster firings and propellant consumption. It is emphasized that the presented method is most beneficial with an automated implementation.

It was further demonstrated that by including the thruster configuration explicitly in the optimization problem, a small propellant saving is achieved. In addition, it was shown that for satellites

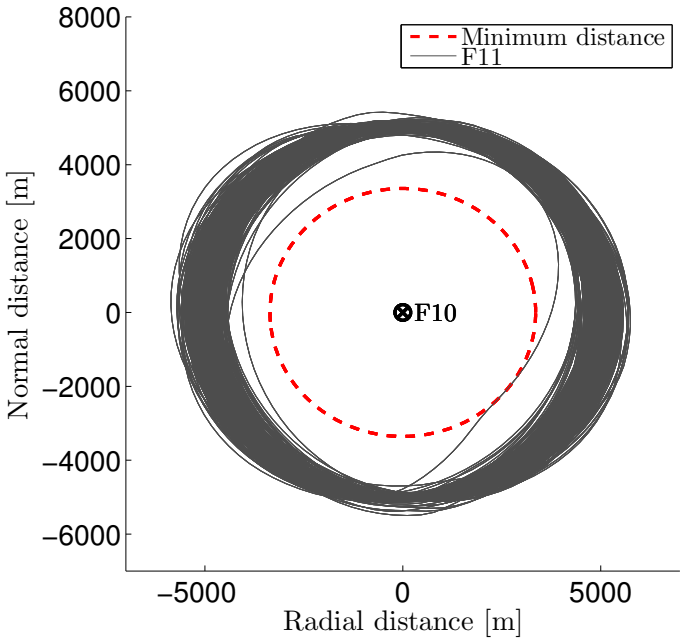

Fig. 11 Relative motion of F11 about F10 in the radial-normal plane.

with typical electric propulsion thruster configurations the classic sun-pointing perigee strategy has no significant advantages in terms of propellant consumption and only limits the eccentricity vector configuration space. Lastly, the thruster configuration has an impact on the orbit prediction and control accuracy and an exemplary configuration with good performance was introduced.

References

[1] Wauthier, P. and Francken, P., "The ASTRA co-location strategy for three to six satellites," *Revista Brasileira de Ciencias Mecanicas (ISSN 0100-7386), vol. 16, p. 163-171*, Vol. 16, 1994, pp. 163–171.

[2] Eckstein, M., Rajasingh, C., and Blumer, P., "Colocation strategy and collision avoidance for the geostationary satellites at 19 degrees west," *International Symposium on Space Flight Dynamics*, 1989.

[3] Wauthier, P., Francken, P., and Laroche, H., "Co-location of six ASTRA satellites: Assessment after one year of operations," *Proceedings of the 12th International Symposium on Space Flight Dynamics*, European Space Agency, 1997, p. 13.

[4] D'Amico, S. and Montenbruck, O., "Proximity Operations of Formation-Flying Spacecraft Using an Eccentricity/Inclination Vector Separation," *Journal of Guidance, Control, and Dynamics*, Vol. 29, No. 3, may 2006, pp. 554–563. doi:10.2514/1.15114.

[5] Beigelman, I. and Gurfil, P., "Optimal Geostationary Satellite Collocation Using Relative Orbital

Element Corrections," *Journal of Spacecraft and Rockets*, Vol. 46, No. 1, jan 2009, pp. 141–150. doi:10.2514/1.35160.

[6] Rausch, R. R., *Relative Orbit Control or Collocated Geostationary Spacecraft*, Ph.D. thesis, Purdue University, 2012.

[7] Acikmese, B., Scharf, D., Hadaegh, F., and Murray, E., "A Convex Guidance Algorithm for Formation Reconfiguration," *AIAA Guidance, Navigation, and Control Conference and Exhibit*, American Institute of Aeronautics and Astronautics (AIAA), aug 2006. doi:10.2514/6.2006-6070.

[8] Morgan, D., Chung, S.-J., and Hadaegh, F. Y., "Model Predictive Control of Swarms of Spacecraft Using Sequential Convex Programming," *Journal of Guidance, Control, and Dynamics*, Vol. 37, No. 6, nov 2014, pp. 1725–1740. doi:10.2514/1.g000218.

[9] de Bruijn, F. J., Theil, S., Choukroun, D., and Gill, E., "Geostationary Satellite Station-Keeping Using Convex Optimization," *Journal of Guidance, Control, and Dynamics*, aug 2015, pp. 1–12. doi:10.2514/1.g001302.

[10] Eckstein, M., "Geostationary orbit control considering deterministic cross coupling effects," *Proceedings of the 41st International Astronautical Federation (IAF) Congress*, IAF, 1990.

[11] Montenbruck, O. and Gill, E., *Satellite Orbits*, Springer Berlin Heidelberg, 2000. doi:10.1007/978-3-642-58351-3.

[12] Schaub, H. and Junkins, J., *Analytical Mechanics Of Space Systems*, American Institute of Aeronautics and Astronautics, jan 2003. doi:10.2514/4.861550.

[13] Chasset, C., Bodin, P., Neumann, N., Larsson, R., and Edfors, A., "Evolution of the AOCS design for EDRS and the satellites of the Small GEO family," *Proceedings of the 9th International ESA Conference on Guidance, Navigation and Control*, ESA, 2014.

[14] Blumer, P., "A future concept of coordinated orbit control of colocated geostationary satellites," *Astrodynamics Conference*, American Institute of Aeronautics and Astronautics (AIAA), aug 1992. doi:10.2514/6.1992-4654.

[15] D'Amico, S, *Autonomous Formation Flying in Low Earth Orbit*, Ph.D. thesis, Delft University of Technology, 2010.

[16] Soop, E. M., *Handbook of Geostationary Orbits*, Microcosm and Kluwer, 1994. doi:10.1007/978-94-015-8352-7.

[17] Betts, J., "Very low-thrust trajectory optimization using a direct {SQP} method," *Journal of Computational and Applied Mathematics*, Vol. 120, No. 1-2, aug 2000, pp. 27–40. doi:10.1016/s0377-0427(00)00301-0.

[18] Boyd, S. and Vandenberghe, L., *Convex Optimization*, Cambridge University Press, 2004. doi:10.1017/cbo9780511804441.

[19] Grant, M. and Boyd, S., "CVX: Matlab Software for Disciplined Convex Programming, version 2.0 beta," `http://cvxr.com/cvx`, sep 2013.

[20] Andersen, E., Jensen, B., Jensen, J., Sandvik, R., and Worsøe, U., "MOSEK version 6," Tech. rep., Technical Report TR–2009–3, MOSEK, 2009.

[21] Casaregola, C., "Electric Propulsion for Station Keeping and Electric Orbit Raising on Eutelsat Platforms," *Proceedings of the 34^{th} IEPC*, Electric Rocket Propulsion Society (ERPS), jul 2015.

[22] Chapel, J., Stancliffe, D., Bevacqua, T., Winkler, S., Clapp, B., Rood, T., Gaylor, D., Freesland, D., and Krimchansky, A., "Guidance, navigation, and control performance for the GOES-R spacecraft," *CEAS Space J*, mar 2015. doi:10.1007/s12567-015-0077-1.